Pattern-to-Absorption Prediction for Multilayered Metamaterial Absorber Based on Deep Learning

Jiawen Wang, Caizhi Fan, Yihuan Liao, and Lilin Zhou

***Abstract*— Metamaterial absorbers (MMAs) allow for a wider range of applications than single-layer ones for their multilayered nature, especially in ultrabroadband absorption. However, the design of multilayered MMAs is extremely complicated. Employed deep learning (DL), using a surrogate model to replace the time-consuming full-wave simulations during the design process can greatly improve the design efficiency. In this letter, an efficient approach for constructing the surrogate model of multilayered MMA is proposed. The coding frequency selective surfaces (FSSs) are converted into multichannel images and then amplified to enhance the efficiency of dataset utilization and model training. A convolutional neural network (CNN) is developed as the surrogate model to achieve pattern-to-absorption prediction for the multilayered MMA with a high degree of freedom. Trained on only 18 000 instances with 2^{108} total permutations, the CNN can predict the absorption of the meta-atoms within the frequency range of 1.00–20.00 GHz in 0.05 s with a mean deviation of 0.02144. Our letter provides an efficient way to construct surrogate models for multilayered MMA in the DL-based design process.**

***Index Terms*— Deep learning (DL), digital coding metamaterial, metamaterial absorber (MMA), multilayered absorber.**

I. Introduction

IN VARIOUS fields, such as electromagnetic (EM) compatibility and radar stealth technology, metamaterial absorbers (MMAs) are employed to reduce the reflection of EM waves [1], [2], [3]. Multiple layers can introduce additional resonances, resulting in multilayered MMAs allowing for a wider range of applications than single-layer ones, especially in ultrabroadband absorption [4], [5], [6]. However, the design complexity is also significantly increased. The conventional approach to designing EM structures requires specialized knowledge and involves multiple iterations, costing plenty of time and computational resources.

To improve the efficiency of designing EM structures, such as MMAs, deep learning (DL) is applied in the design process [7], [8], [9], [10], [11]. According to the different input–output relationships of data-driven models, DL-based design can be categorized into direct inverse design based on the response-structure (R-S) model [12], [13], [14], [15] and inverse design based on the structure-response (S-R) surrogate model [16], [17]. Compared to the R-S model, the S-R surrogate model mitigates the issues related to training difficulties arising from the one-to-many correspondence between EM responses and EM structures. In the design process, the S-R surrogate model is employed to characterize the relationship between EM structures and EM response, and then time-consuming modeling and simulation are avoided. Therefore, the construction of the S-R surrogate model is vital. Training the S-R surrogate model is a one-time process; however, it often requires a substantial amount of data, especially for structures with high design complexity [18]. Currently, the S-R surrogate model construction mainly focuses on the singer-layer EM structures and the structures with a small number of parameters [19], [20], [21], [22], in which design complexity is reduced but its application is also limited. Multilayered MMAs show superiority in meeting distinct design targets due to their great flexibility. However, the surrogate model meets training inefficiency for the high dimension of input design parameters. The research on multilayered EM structures that retain a high degree of freedom is still lacking.

In this letter, we proposed an approach for constructing the S-R surrogate model of the multilayered MMA with a high degree of freedom based on DL. The features are input through multichannels to the S-R surrogate model. The training efficiency is enhanced by amplifying the encoded information of the designed meta-atom. The simulation results of the S-R surrogate model are illustrated to verify the effectiveness and superiority.

II. Design of Meta-Atom

As shown in Fig. 1(a), the meta-atom, the component of multilayered MMA, consists of three lossy layers, and the consecutive layers are separated by air spacers. Resistive films are maintained into patterns and printed on FR-4 sheets ($\varepsilon_r = 4.4$, $\tan\theta = 0.02$), where ε_r represents relative permittivity and $\tan\theta$ means loss tangent. And the meta-atom is backed by an aluminum plate to make transmission zero. All frequency-selective surfaces (FSSs) are encoded using the same rules. Fig. 1(b) illustrates the digital coding rule of the FSSs for the meta-atom, each FSS is discretized into $N \times N$ uniform squares. Each small grid is filled with either 0 or 1, where "1" is covered with resistive film and "0" is not. In the interest of reducing the effects of polarization, the FSSs are designed to have fourfold symmetry, resulting in the $N \times N$ matrices being represented by $N/2 \times N/2$ matrices.

Manuscript received 21 January 2024; revised 4 March 2024; accepted 3 April 2024. Date of publication 16 April 2024; date of current version 10 May 2024. This work was supported in part by the Hunan Provincial Natural Science Foundation of China under Grant 2022JJ40544 and in part by the National Natural Science Foundation of China under Grant 12202484. *(Corresponding author: Yihuan Liao.)*

The authors are with the College of Aerospace Science and Engineering, National University of Defense Technology, Changsha 410073, China (e-mail: wangjiawen21@nudt.edu.cn; caizhifan@nudt.edu.cn; 13548599641@139.com; zllftx@nudt.edu.cn).

Color versions of one or more figures in this letter are available at https://doi.org/10.1109/LMWT.2024.3385982.

Digital Object Identifier 10.1109/LMWT.2024.3385982

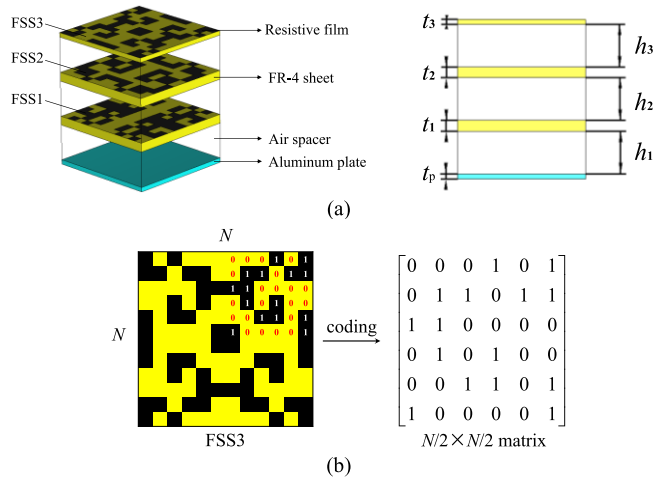

Fig. 1. (a) Schematic of the multilayered lossy meta-atom. (b) Schematic of FSSs discrete coding rule.

In this letter, the sheet resistance of the resistive films is 50 Ω/sq. The geometrical parameters of the meta-atom are as follows, $t_1 = 1$ mm, $t_2 = 1$ mm, $t_3 = 0.5$ mm, $h_1 = h_2 = h_3 = 4$ mm, $t_p = 0.5$ mm, and the periodicity is 12 mm. And N is set to 12. Therefore, the features of meta-atom can be represented using three 6×6 binary matrices, indicating 2^{108} possible permutations, making it challenging to simulate all possible combinations and establish the relationship between the feature matrices and EM response directly.

III. Dataset Construction and Preprocessing

Since a significant of training instances is necessary, MATLAB-CST co-simulation is employed to prepare the dataset. In the first place, MATLAB is used to arbitrarily generate three binary matrices. Subsequently, CST models the corresponding MMA structure and simulates it automatically at the normal incidence of waves with unit cell boundary by employing a frequency domain solver, which takes about 50 s for every single EM simulation. Then, the three binary matrices and the corresponding reflection coefficient are stored and added to the dataset. Finally, we collected 20 000 samples as the dataset, which took 12 days.

In order to establish the mapping relationship from input features to output EM response using smaller sample datasets, data preprocessing is required. To accurately represent the feature of the FSSs, we perform axisymmetric transformations on the randomly generated 6×6 matrices to restore them as 12×12 matrices. Each layer of FSS can be characterized as a single-channel image, then the meta-atoms can be further characterized as a three-channel binary image. Due to the small image pixel size, the complexity of the surrogate model is limited. To further enhance the performance of the surrogate model and increase the complexity of the feasible network while avoiding redundant information, we enlarge the images to twice their original size, resulting in the input three-channel binary images with pixel dimensions of 24×24. And the output absorption of the MMA can be calculated by the simulated S-parameters. The presence of the metal plate on the backside of the structure blocks transmission, allowing the absorptivity to be calculated by

$$A(\omega) = 1 - |S_{11}|^2 \tag{1}$$

where S_{11} represents the reflection coefficient. The corresponding absorptivity obtained from EM simulation-based CST is 1001-dimension, which makes it extremely hard to train the model. We shrink the original absorptivity by sampling for about every 0.6 GHz, and finally, get the 35-dimensional features.

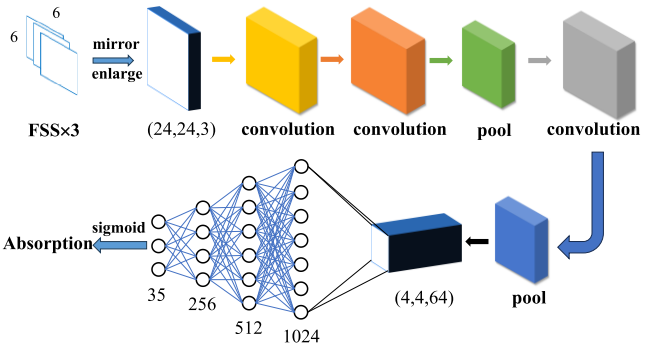

Fig. 2. Schematic illustration of the CNN structure.

After data preprocessing, the prediction for the EM response of meta-atoms is modeled as a regression problem from three-channel images with a pixel size of 24×24 to 35-dimensional data. The local characteristics of FSSs determine the EM response of the meta-atoms at distinct frequencies. Therefore, a convolutional neural network (CNN) is applied to construct the surrogate model.

IV. Construction of S-R Surrogate Model

After data preprocessing, the shape of the input tensor is [24, 24, 3], where the parameters correspond to the horizontal dimension H, the vertical dimension W, and the depth C of the input tensor. The detailed architecture of the CNN is illustrated in Fig. 2.

As shown in Fig. 2, the developed CNN mainly consists of three convolutional layers, two pooling layers, and three fully connected layers. The three convolutional layers with a kernel size of 3×3 and the pooling layers use max pooling with a pool size of 2×2. While the other fully connected layers and convolutional layers use LeakyReLU as the activation function, Sigmoid is selected for the last fully connected layer to ensure that the output results are always between 0 and 1 according to our targets, the definition is as follows:

$$\text{Sigmoid}(x) = \frac{1}{1 + e^{-x}}. \tag{2}$$

To measure the predicting accuracy for the regression problem, MSE is taken as the loss function

$$L = \frac{1}{N} \sum_{i=1}^{N} (y_{\text{pred}} - y)^2 \tag{3}$$

where y_{pred} and y are 35-dimensional vectors, and represent the predicted and the simulated absorptivity, respectively.

Among the dataset, 18 000 samples from the dataset are used to train the model, 1000 are used to validate the

model, and the rest 1000 are used to test to evaluate the generalization ability of the model. The CNN is built by PyTorch 1.8.1+cu111 in Python 3.7.16. We set an initial learning rate of 0.002 for the model, and the learning rate is discretely adjusted downward. And we chose Adam optimizer. Moreover, squeeze-and-excitation (SE) blocks are introduced. SE blocks include global information embedding and adaptive recalibration, as illustrated as follows:

$$z_c = F_{\text{eq}}(X) = \frac{1}{H \times W} \sum_{i=1}^{H} \sum_{j}^{W} X(i, j) \tag{4}$$

$$Y = \sigma(F_{\text{ex}}(z_c)) \odot X \tag{5}$$

where X and Y represent input and output, F_{eq} denotes global average pooling, resulting in z_c being a tensor with a shape of $1 \times 1 \times C$, F_{ex} means fully connected layers, $\odot$ represents a weighting of the original features, and σ is the activation function. We adapt the reduction ratio carefully to ensure that the constructed CNN focuses on the more critical channels for the current task and suppresses the channels with smaller relevance. Trained after 120 epochs for several minutes with a batch size of 96 samples, the model converged to an MSE loss of around 7.2×10^{-4}. To characterize the performance of the trained model, MAE, which is also called mean deviation, is set as the evaluation metric and given by

$$D = \frac{1}{35} \sum_{i=1}^{35} \left| A_p(i) - A_s(i) \right| \tag{6}$$

where A_p is the predicted absorptivity and A_s is the real value.

To have a more intuitive impression of the predictive ability of the model, we randomly selected several instances from the test dataset and compared the predicted and real values of absorption. As shown in Fig. 3, the predicted absorption trend is close to the simulated results for MMAs with different EM response characteristics, indicating the model performs excellent predictive ability. Compared to the 50 s required for EM simulation, the trained CNN carries out the absorptivity in just 0.05 s, which is only one-thousandth of the EM simulation. The average MAE of the whole test dataset is 0.02144, and the proportion with an MAE lower than 0.03 is 85.1%. To validate the effectiveness of feature enlargement, we also constructed a model to train data without enlarged features and trained for the same epochs. The model performance of the feature with and without enlargement is compared in Table I. By enlarging the data features and constructing a more complex CNN model, the final loss function decreased by 67%, the average deviation decreased by 20%, and the proportion of samples with an MAE lower than 0.03 increased by 18.2%.

Using the effective prediction of EM response as the criterion, the total permutations and required training samples of S-R models in prior work are compared in Table II. Compared to the prior work, the design of multilayered MMAs in this study exhibits significantly increased complexity and flexibility. Table II illustrates that the effective prediction of the EM response of metamaterials is achieved with the fewest training samples in this work while the number of total permutations is the largest, validating the efficiency of the proposed S-R surrogate model construction approach.

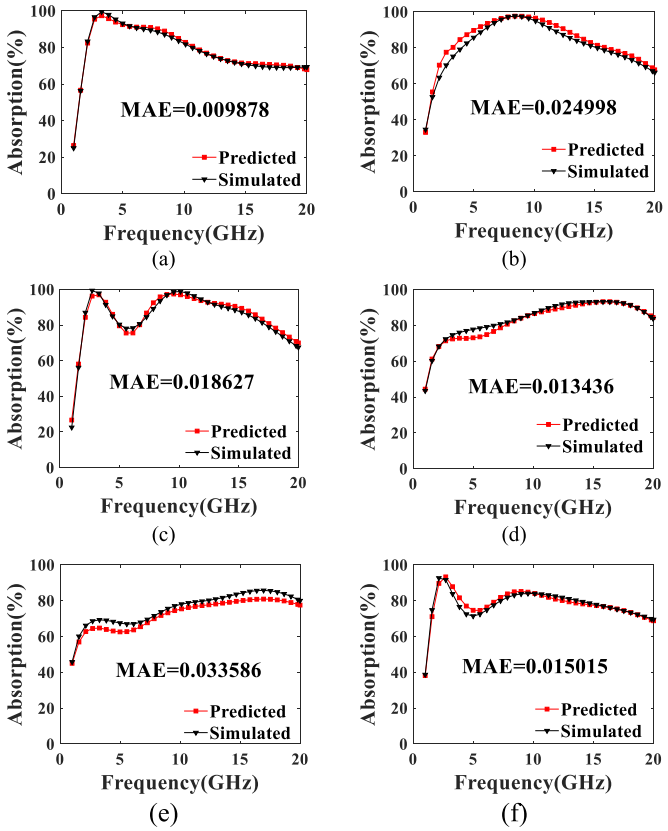

Fig. 3. Absorption obtained by CNN and simulation. (a)–(e) Well predicted with MAE below 0.03. (f) Similar trend with MAE above 0.03.

TABLE I
EFFECTIVENESS VALIDATION OF ENLARGING FEATURE

feature	input tensor shape	MSE loss	average MAE (test dataset)	MAE below 0.03
original	[12,12,3]	2.2×10^{-3}	0.02678	66.9%
enlarged	[24,24,3]	7.2×10^{-4}	0.02144	85.1%

TABLE II
S-R MODELS OF METAMATERIALS

FSS layer	FSS form	total permutations	training samples	reference
single	topological	2^{64}	20,000	[16]
single	topological	2^{64}	70,000	[22]
triple	topological	2^{108}	18,000	this work

V. CONCLUSION

A surrogate model construction approach for absorption prediction of multilayered MMA is proposed in this letter. The efficiency of the proposed method is demonstrated through full-wave simulations of structures with distinct EM responses. The effectiveness of amplifying features is validated through the comparison of the enlarged ones and the original ones. After training, the surrogate model can provide the absorptivity within 0.05 s. Compared to the prior work, the surrogate model effectively predicts the corresponding EM response using a relatively smaller dataset while the complexity of the EM structure is significantly increased.

REFERENCES

[1] G. Deng, Z. Yu, J. Yang, Z. Yin, Y. Li, and B. Chi, "A miniaturized 3-D metamaterial absorber with wide angle stability," *IEEE Microw. Wireless Compon. Lett.*, vol. 32, no. 9, pp. 1111–1114, Sep. 2022.

[2] Y. Fang, K. Pan, T. Leng, H. H. Ouslimani, K. S. Novoselov, and Z. Hu, "Controlling graphene sheet resistance for broadband printable and flexible artificial magnetic conductor-based microwave radar absorber applications," *IEEE Trans. Antennas Propag.*, vol. 69, no. 12, pp. 8503–8511, Dec. 2021.

[3] T. Shi, M.-C. Tang, J. Yang, and X. Yuan, "A low-profile and ultrawideband capacitive circuit absorber empowered by enlarged unit periodicity," *IEEE Antennas Wireless Propag. Lett.*, vol. 21, no. 3, pp. 551–555, Mar. 2022.

[4] Y. Tayde, M. Saikia, K. V. Srivastava, and S. A. Ramakrishna, "Polarization-insensitive broadband multilayered absorber using screen printed patterns of resistive ink," *IEEE Antennas Wireless Propag. Lett.*, vol. 17, no. 12, pp. 2489–2493, Dec. 2018.

[5] M. Guo et al., "Broadband absorptive frequency-selective rasorber based on multilayer resistive sheets using multilayer resonator," *IEEE Trans. Antennas Propag.*, vol. 70, no. 3, pp. 2009–2022, Mar. 2022.

[6] H. W. Lan et al., "Low-frequency broadband multilayer microwave metamaterial absorber based on resistive frequency selective surfaces," *Appl. Opt.*, vol. 62, no. 4, pp. 1096–1102, Jan. 2023.

[7] W. Ma, Z. Liu, Z. A. Kudyshev, A. Boltasseva, W. Cai, and Y. Liu, "Deep learning for the design of photonic structures," *Nature Photon.*, vol. 15, no. 2, pp. 77–90, Feb. 2021.

[8] W. Li et al., "Deep learning modeling strategy for material science: From natural materials to metamaterials," *J. Phys., Mater.*, vol. 5, no. 1, Mar. 2022, Art. no. 014003.

[9] B. Wang, C. Xu, G. Duan, W. Xu, and F. Pi, "Review of broadband metamaterial absorbers: From principles, design strategies, and tunable properties to functional applications," *Adv. Funct. Mater.*, vol. 33, no. 14, Apr. 2023, Art. no. 2213818.

[10] J. Parmar, S. K. Patel, and V. Katkar, "Graphene-based metasurface solar absorber design with absorption prediction using machine learning," *Sci. Rep.*, vol. 12, no. 1, Feb. 2022, Art. no. 2609.

[11] S. Krasikov, A. Tranter, A. Bogdanov, and Y. Kivshar, "Intelligent metaphotonics empowered by machine learning," *Opto-Electron. Adv.*, vol. 5, no. 3, p. 210147, 2022.

[12] T. Qiu et al., "Deep learning: A rapid and efficient route to automatic metasurface design," *Adv. Sci.*, vol. 6, no. 12, Apr. 2019, Art. no. 1900128.

[13] X. Shi, T. Qiu, J. Wang, X. Zhao, and S. Qu, "Metasurface inverse design using machine learning approaches," *J. Phys. D, Appl. Phys.*, vol. 53, no. 27, Jul. 2020, Art. no. 275105.

[14] X. Lu et al., "Classification and inverse design of metasurface absorber in visible band," *Adv. Theory Simulations*, vol. 5, no. 3, Mar. 2022, Art. no. 2100338.

[15] V. Chaudhary and R. Panwar, "Machine learning empowered magnetic substrate coupled broadband and miniaturized frequency selective surface," *IEEE Trans. Electromagn. Compat.*, vol. 65, no. 2, pp. 406–413, Apr. 2023.

[16] R. Zhu et al., "Phase-to-pattern inverse design paradigm for fast realization of functional metasurfaces via transfer learning," *Nature Commun.*, vol. 12, no. 1, May 2021, Art. no. 2974.

[17] T. Knightley, A. Yakovlev, and V. Pacheco-Peña, "Neural network design of multilayer metamaterial for temporal differentiation," *Adv. Opt. Mater.*, vol. 11, no. 5, Mar. 2023, Art. no. 2202351.

[18] Q. Ding, G. Wan, N. Wang, and X. Ma, "Dataset shrinking for accelerated deep learning-based metamaterial absorber design," *IEEE Microw. Wireless Technol. Lett.*, vol. 33, no. 8, pp. 1111–1114, Aug. 2023.

[19] J. Chen et al., "Absorption and diffusion enabled ultrathin broadband metamaterial absorber designed by deep neural network and PSO," *IEEE Antennas Wireless Propag. Lett.*, vol. 20, no. 10, pp. 1993–1997, Oct. 2021.

[20] N. Chen, C. He, and W. Zhu, "Lightweight machine-learning model for efficient design of graphene-based microwave metasurfaces for versatile absorption performance," *Nanomaterials*, vol. 13, no. 2, p. 329, Jan. 2023.

[21] W. Ding, J. Chen, and R. Wu, "A generative meta-atom model for metasurface-based absorber designs," *Adv. Opt. Mater.*, vol. 11, no. 2, Jan. 2023, Art. no. 2201959.

[22] Q. Zhang et al., "Machine-Learning designs of anisotropic digital coding metasurfaces," *Adv. Theory Simulations*, vol. 2, no. 2, Feb. 2019, Art. no. 1800132.